Electronic Supplementary Materials

For https://doi.org/10.1631/jzus.A2500501

Wear map-based wear prediction method for the piston–cylinder interface in axial piston machines

Fei LYU[1,2], Xudong SHEN[1], Felix SCHLEGEL[2], Xiaolong ZHANG[1]✉, Liangyu SONG[1], Junhui ZHANG[1], Katharina SCHMITZ[2], Bing XU[1]

[1]State Key Laboratory of Fluid Power & Mechatronic Systems, Zhejiang University, Hangzhou 310058, China
[2]Institute for Fluid Power Drives and Systems (ifas), RWTH Aachen University, Aachen 52074, Germany

Section S1 Lubrication model for PCI

The contact state at the interface can be analyzed starting with the force state between the piston and cylinder bore. Fig. S1 illustrates the schematic diagram of the external forces acting on the piston. During operation, the piston/cylinder assembly experiences complex force states, which can be broadly categorized into two types. The first type of forces are concentrated forces with specific expressions, including the piston chamber hydraulic force $\boldsymbol{F}_{\mathrm{ch}}$, the friction force between the swash plate and the slipper $\boldsymbol{F}_{\mathrm{sf}}$, the supporting force of the slipper on the piston $\boldsymbol{F}_{\mathrm{ss}}$, the centrifugal force F_{c}, gravitational force $\boldsymbol{F}_{\mathrm{g}}$, and inertial force $\boldsymbol{F}_{\mathrm{i}}$ of the piston. In the *OXYZ* coordinate system, the expressions for the concentrated forces acting on the piston are as follows.

The hydraulic force in the piston chamber $\boldsymbol{F}_{\mathrm{ch}}$ is given by:

$$\boldsymbol{F}_{\mathrm{ch}} = \begin{bmatrix} 0 & 0 & p_{\mathrm{ch}}\pi R_{\mathrm{c}}^2 \end{bmatrix}, \tag{S1}$$

where p_{ch} is the piston chamber pressure, R_{c} is the radius of the cylinder bore.

The gravity $\boldsymbol{F}_{\mathrm{g}}$ is given by:

$$\boldsymbol{F}_{\mathrm{g}} = \begin{bmatrix} 0 & -m_{\mathrm{p}}g & 0 \end{bmatrix}, \tag{S2}$$

where m_{p} is the mass of the piston.

The centrifugal force $\boldsymbol{F}_{\mathrm{c}}$, is given by:

$$\boldsymbol{F}_{\mathrm{c}} = \begin{bmatrix} m_{\mathrm{c}}\omega^2 R_{\mathrm{pt}}\sin\varphi & m_{\mathrm{c}}\omega^2 R_{\mathrm{pt}}\cos\varphi & 0 \end{bmatrix}, \tag{S3}$$

where R_{pt} is the pitch radius of the piston, ω is the shaft speed, φ is the shaft angle.

The inertial force of the piston $\boldsymbol{F}_{\mathrm{i}}$ is given by:

$$\boldsymbol{F}_{\mathrm{i}} = \begin{bmatrix} 0 & 0 & -m_{\mathrm{p}}a_{\mathrm{p}} \end{bmatrix}, \tag{S4}$$

where a_{p} is the acceleration of the piston, i.e., the derivative of the reciprocating sliding velocity v_z.

The friction force between the swash plate and the slipper $\boldsymbol{F}_{\mathrm{sf}}$ is given by:

$$\boldsymbol{F}_{\mathrm{sf}} = \begin{bmatrix} -f_{\mathrm{s}}F_{\mathrm{ss}}\cos\varphi & f_{\mathrm{s}}F_{\mathrm{ss}}\sin\varphi & 0 \end{bmatrix}, \tag{S5}$$

where f_{s} is the average frictional coefficient between the slipper and the swash plate, and it is set to 0.03, and F_{ss} is the magnitude of the unknown supporting force of the slipper on the piston, which is temporarily represented by the symbol and will be analyzed as follows. The supporting force $\boldsymbol{F}_{\mathrm{ss}}$ cannot be directly solved but can be expressed by the force equilibrium in the Z direction:

$$\boldsymbol{F}_{\mathrm{ss}} = \begin{bmatrix} 0 & \left(\boldsymbol{F}_{\mathrm{po\_z}} + \boldsymbol{F}_{\mathrm{ps\_z}} + \boldsymbol{F}_{\mathrm{i\_z}} + \boldsymbol{F}_{\mathrm{c\_z}} + \boldsymbol{F}_{\mathrm{pf\_z}} + \boldsymbol{F}_{\mathrm{ch\_z}}\right)\tan\gamma & \boldsymbol{F}_{\mathrm{po\_z}} + \boldsymbol{F}_{\mathrm{ps\_z}} + \boldsymbol{F}_{\mathrm{i\_z}} + \boldsymbol{F}_{\mathrm{c\_z}} + \boldsymbol{F}_{\mathrm{pf\_z}} + \boldsymbol{F}_{\mathrm{ch\_z}} \end{bmatrix}, \tag{S6}$$

where γ is the inclined angle of the swash plate. This expression can be used in the equilibrium equations as shown in Eq. (S7).

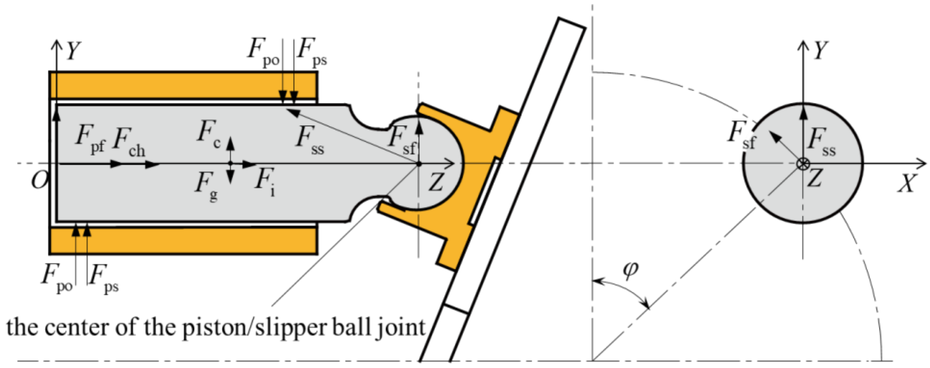

Fig. S1 Force state of the PCI

The second type of forces, which are more complicated, are distributed along the piston surface. Their expression requires the bearing and lubrication parameters of the PCI clearance. They are the supporting force of the oil film on the piston $\boldsymbol{F}_{po}$, the solid contact supporting force of the cylinder bore on the piston $\boldsymbol{F}_{ps}$, and the friction force between the piston and the cylinder bore $\boldsymbol{F}_{pf}$. The force and moment equilibrium equations of the piston are shown in Eq.(S7):

$$\begin{cases} \boldsymbol{F}_e = \boldsymbol{F}_{ch} + \boldsymbol{F}_{sf} + \boldsymbol{F}_{ss} + \boldsymbol{F}_c + \boldsymbol{F}_g + \boldsymbol{F}_i + \boldsymbol{F}_{po} + \boldsymbol{F}_{ps} + \boldsymbol{F}_{pf} \\ \boldsymbol{M}_e = \boldsymbol{M}_{po} + \boldsymbol{M}_{ps} + \boldsymbol{F}_c \cdot L_m + \boldsymbol{F}_g \cdot L_m \end{cases}, \tag{S7}$$

where $\boldsymbol{F}_e$ and $\boldsymbol{M}_e$ are the resultant force vector and resultant moment vector, respectively, L_m is the distance between the barycenter and the center of the piston/slipper ball joint, $\boldsymbol{M}_{po}$ and $\boldsymbol{M}_{ps}$ are the moments of $\boldsymbol{F}_{po}$ and $\boldsymbol{F}_{ps}$ with respect to the center of the piston/slipper ball joint, respectively. Forces and moments in Eq. (S7) are 1×3 vectors, in which the elements represent the components of the force in the X, Y and Z direction, respectively. As long as all the forces applied on the piston being expressed, the distributed solid contact stress can be obtained by solving the force and moment equilibrium equations of the piston.

The supporting force of the oil film on the piston, $\boldsymbol{F}_{po}$ is determined by the oil film pressure p_o, which can be described by the Reynolds equation:

$$\frac{1}{R_c^2}\frac{\partial}{\partial\theta}\left(\phi_\theta \frac{h_o^3}{\mu}\frac{\partial p_o}{\partial\theta}\right) + \frac{\partial}{\partial z}\left(\phi_z \frac{h_o^3}{\mu}\frac{\partial p_o}{\partial z}\right) = 6\left(v_\theta \frac{1}{R_c}\left(\frac{\partial h_o}{\partial\theta} + \sigma\frac{\partial\phi_{s\theta}}{\partial\theta}\right) + v_z\left(\frac{\partial h_o}{\partial z} + \sigma\frac{\partial\phi_{sz}}{\partial z}\right) + 2\frac{\partial h_o}{\partial t}\right), \tag{S8}$$

where h_o is the oil film thickness, R_c is the radius of the cylinder bore, ϕ_θ and ϕ_z are the pressure flow factors in the circumferential direction and that in the axial direction, respectively, $\phi_{s\theta}$ and ϕ_{sz} are the shear flow factors(Patir and Cheng 1978), σ is the root mean square roughness of the piston surface(Lyu et al. 2023), μ is the dynamic viscosity of the oil, which is incorporated through an induced-pressure transformation based on the Chu-Cameron pressure-viscosity relationship (Chu and Cameron 1962, Gohar and Cameron 1967). It should be noted that thermal effects are not considered in the present model, and the lubricant temperature is assumed to be constant. v_θ is circumferential sliding velocity between the piston and the cylinder bore which is related to the spin of the piston (Chao et al. 2018, Ransegnola et al. 2022), v_z is the reciprocating sliding velocity which is calculated by Eq. (S9):

$$v_z = R_{pt}\omega\tan\gamma\sin\varphi, \tag{S9}$$

where R_{pt} is the pitch radius of the piston, ω is the shaft speed, γ is the inclined angle of the swash plate, φ is the shaft angle.

Since the Reynolds equation is a second-order partial differential equation with a source term, it requires numerical solutions. The Reynolds equation is discretized using the finite difference method (FDM) on a structured grid, and the resulting algebraic equations are solved iteratively, as detailed in Appendix B. The grid area is A_g, and then the local F_{po} can be expressed as:

$$F_{po}\left(\theta,z\right)=p_o\left(\theta,z\right)A_g. \tag{S10}$$

The supporting force of solid contact, $\boldsymbol{F}_{ps}$ is determined by the elastic contact stress between the piston and the cylinder bore p_s, which can be expressed as:

$$p_s\left(\theta,z\right)=\Delta h\left(\theta,z\right)\cdot k_e, \tag{S11}$$

where k_e is the equivalent contact stiffness of the PCI. It can be calculated by Eq.(S12)(Singh et al. 2021):

$$k_e=\frac{R_c\left(1+\nu_p\right)}{E_p}+\frac{R_c}{E_c}\frac{\left(1-\nu_c\right)\left(R_c+H_c\right)^2+\left(1+\nu_c\right)R_c^{\ 2}}{H_c^{\ 2}+2R_cH_c}, \tag{S12}$$

where E_p and E_c are the elasticity modulus of the piston and the cylinder bore respectively, ν_p and ν_c are the Poisson's ratio of the piston and the cylinder bore respectively, H_c is the thickness of the cylinder block in the radial direction, and Δh is the contact depth, which is related to the tilting posture of the piston within the cylinder bore which can be quantitatively represented by the eccentricity $\boldsymbol{e}$ of the piston center relative to the cylinder bore at the two axial boundary cross sections of the oil film. Here, e_1 and e_2 are the eccentricities in the X-direction at the two cross sections, and e_3 and e_4 are the eccentricities in the Y-direction at the two cross sections. The lubrication simulation is conducted based on an ideal cylindrical interface between the piston and the cylinder bore.

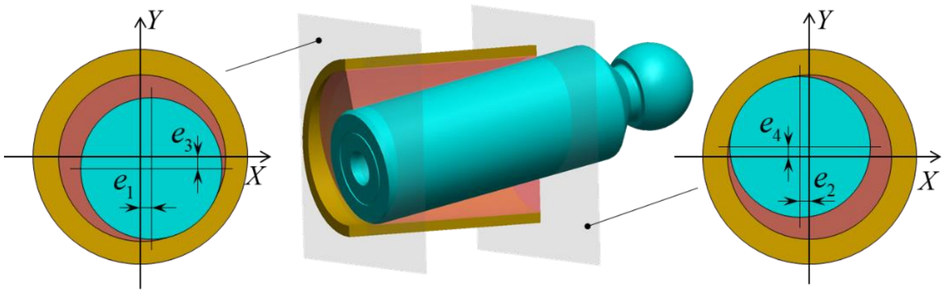

Fig. S2 Tilting and eccentricity of the piston

Based on geometric relationships, the contact depth Δh can ideally be expressed by the eccentricity, as shown in Eq.(S13):

$$\Delta h\left(\theta,z\right)=\begin{cases}0 & h_e\left(\theta,z\right)\geq h_m\\ h_m-h_e\left(\theta,z\right) & h_e\left(\theta,z\right)\geq h_m\end{cases}, \tag{S13}$$

in which the intermediate variable h_e is defined as:

$$h_e\left(\theta,z\right)=\left(R_c-R_p\right)-\left(e_1-\frac{e_1z-e_2z}{L_c}\right)\cos\theta-\left(e_3-\frac{e_3z-e_4z}{L_c}\right)\sin\theta+h_w\left(\theta,z\right), \tag{S14}$$

where h_w is the wear depth, h_m is the minimum oil film thickness, which is simplistically assumed to be determined by the root mean square roughness of the piston and cylinder bore (Mizell 2018, Sarode et al. 2022). Then the local solid contact supporting force F_{ps} at point (θ, z) can be calculated as:

$$F_{ps}\left(\theta,z\right)=p_s\left(\theta,z\right)A_g. \tag{S15}$$

The friction force $\boldsymbol{F}_{pf}$ consists of viscous friction of the oil film and solid contact friction. Among these, the viscous friction is determined by the viscous shear stress on the piston surface, τ, which is calculated by the Newtonian friction law, as shown in Eq. (S16):

$$\tau\left(\theta,z\right)=\mu\frac{v_s}{h_o\left(\theta,z\right)}. \tag{S16}$$

In this equation, v_s is the resultant sliding speed between the piston and the cylinder which is calculated by the reciprocating velocity v_z and the spin velocity v_θ as:

$$v_{s} = \sqrt{{v_z}^2 + {v_\theta}^2} . \tag{S17}$$

The viscous friction force can be calculated as the product of the viscous shear stress of the oil film and the corresponding grid area A_g. The solid contact friction is calculated by the same approach. Therefore, the local friction force at the PCI can be expressed as:

$$F_{pf}\left(\theta, z\right) = \left[\tau\left(\theta, z\right) + f_p p_s\left(\theta, z\right)\right] A_g , \tag{S18}$$

where f_p is the dynamic friction coefficient between the piston and the cylinder bore.

The oil film supporting force of the PCI is generated through the reciprocating motion and tilting micro-motion of the piston within the cylinder bore. The solid contact force of the PCI is also determined based on the contact state of the piston. To achieve force balance, the piston must continuously adjust its position within the cylinder bore to obtain appropriate oil film supporting force and solid contact supporting force. After all the concentrated and distributed forces in force equilibrium equation of the piston are explicitly expressed, Eq. (S7), the force and moment equilibrium equations of the PCI can be solved. The oil film supporting force arises from the reciprocating motion and tilting micro-motion of the piston within the cylinder bore, while the solid contact supporting force depends on the contact state of the PCI. Therefore, to achieve the equilibrium, the piston continuously adjusts its position within the cylinder bore to obtain appropriate oil film and solid contact supporting forces. The Newton-Raphson method is adopted to iteratively solve Eq. (S7). With specified initial values, the position of the piston and its variation can be represented by the shifting rates of the eccentricities of the piston cross section centers $\dot{\boldsymbol{e}}$, which are the iteration variables during the iterative process. the Newton-Raphson method can express the equilibrium equations $f\left(\dot{\boldsymbol{e}}\right)$ as

$$f\left(\dot{\boldsymbol{e}}^n\right) = -f'\left(\dot{\boldsymbol{e}}^n\right)\cdot\left(\dot{\boldsymbol{e}}^{n+1} - \dot{\boldsymbol{e}}^n\right), \tag{S19}$$

where n is the iteration step index. The Jacobian matrix of Eq. (S19) is given by Eq. (S20):

$$\mathrm{J}(\dot{\boldsymbol{e}}^n) = f'(\dot{\boldsymbol{e}}^n) = \begin{bmatrix} \dfrac{\partial F_x(\dot{\boldsymbol{e}}^n)}{\partial \dot{e}_1^n} & \dfrac{\partial F_x(\dot{\boldsymbol{e}}^n)}{\partial \dot{e}_2^n} & \dfrac{\partial F_x(\dot{\boldsymbol{e}}^n)}{\partial \dot{e}_3^n} & \dfrac{\partial F_x(\dot{\boldsymbol{e}}^n)}{\partial \dot{e}_4^n} \\ \dfrac{\partial F_y(\dot{\boldsymbol{e}}^n)}{\partial \dot{e}_1^n} & \dfrac{\partial F_y(\dot{\boldsymbol{e}}^n)}{\partial \dot{e}_2^n} & \dfrac{\partial F_y(\dot{\boldsymbol{e}}^n)}{\partial \dot{e}_3^n} & \dfrac{\partial F_y(\dot{\boldsymbol{e}}^n)}{\partial \dot{e}_4^n} \\ \dfrac{\partial M_x(\dot{\boldsymbol{e}}^n)}{\partial \dot{e}_1^n} & \dfrac{\partial M_x(\dot{\boldsymbol{e}}^n)}{\partial \dot{e}_2^n} & \dfrac{\partial M_x(\dot{\boldsymbol{e}}^n)}{\partial \dot{e}_3^n} & \dfrac{\partial M_x(\dot{\boldsymbol{e}}^n)}{\partial \dot{e}_4^n} \\ \dfrac{\partial M_y(\dot{\boldsymbol{e}}^n)}{\partial \dot{e}_1^n} & \dfrac{\partial M_y(\dot{\boldsymbol{e}}^n)}{\partial \dot{e}_2^n} & \dfrac{\partial M_y(\dot{\boldsymbol{e}}^n)}{\partial \dot{e}_3^n} & \dfrac{\partial M_y(\dot{\boldsymbol{e}}^n)}{\partial \dot{e}_4^n} \end{bmatrix}. \tag{S20}$$

The partial derivatives in the Jacobian matrix are computed using finite difference forms as detailed in Appendix B. A convergence tolerance T_e is defined for the Newton-Raphson method. When the force imbalance falls below the allowable deviation, the iterative process terminates, and the converged $\dot{\boldsymbol{e}}^{n+1}$ are output. Through this solution procedure, the concentrated and distributed forces acting on the piston, as well as the contact states and lubrication conditions at the PCI, can be obtained. The flowchart of the iterative solution is schematically illustrated in Fig. S3.

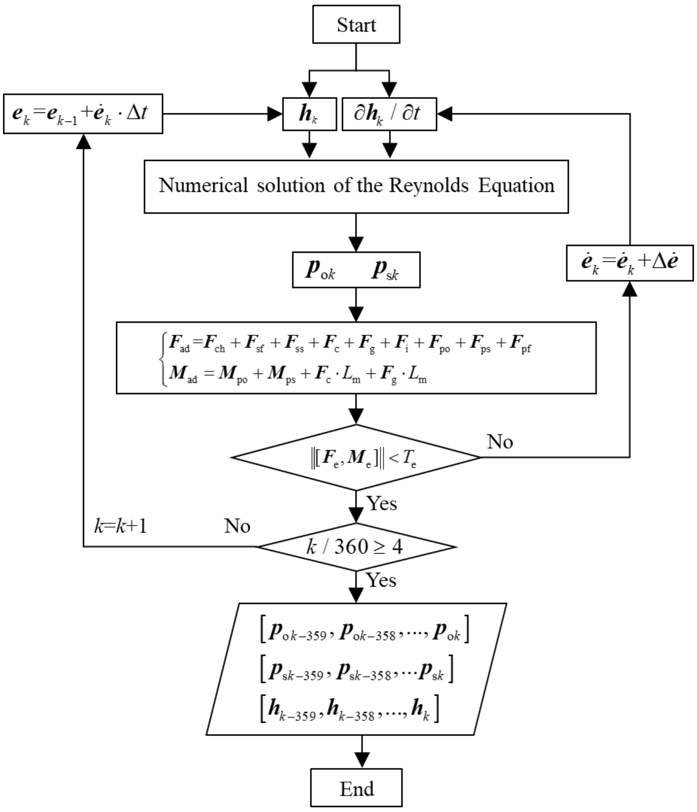

Fig. S3 Schematic flowchart of PCI equilibrium iterative solution

In each analysis step, the distribution of the contact stress which satisfies Eq. (S21) can be output.

$$\|[\boldsymbol{F}_e, \boldsymbol{M}_e]\| < T_e, \tag{S21}$$

where T_e is the tolerance for the residual of the equilibrium.

The mixed lubrication model described in this section is implemented using an in-house code developed in MATLAB. In the present study, thermal effects and pressure-induced elastic deformation of the piston and cylinder bore are not included.

Section S2 Solving the Reynolds Equation of the PCI

The Reynolds equation as shown in Eq. (S8), which characterizes the lubrication condition at the PCI, is a partial differential equation (PDE) with source and diffusion terms. Numerical computation method is required to solve it. With the film thickness prescribed as a known input, the Reynolds equation is transformed into the standard form of a two-dimensional, second-order PDE:

$$A\frac{\partial^2 p_o}{\left[\partial\left(R_c\theta\right)\right]^2} + B\frac{\partial^2 p_o}{\partial z^2} + C\frac{\partial p_o}{\partial\left(R_c\theta\right)} + D\frac{\partial p_o}{\partial z} = E. \tag{S22}$$

The finite difference method (FDM) is adopted to discretize the Reynolds equation of the PCI. Based on the principles of finite differences, the first- and second-order partial derivatives of the oil film pressure p_o at a specific location can be represented by the values of adjacent nodes p_E, p_S, p_W and p_N, as illustrated in Fig. S4.

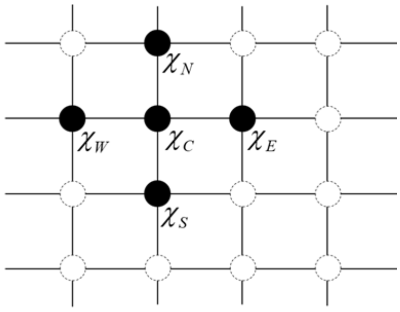

Fig. S4 Schematic diagram of finite difference relations

Then the partial derivatives of the pressure p_{o} can be approximated by p_{E}, p_{S}, p_{W} and p_{N}:

$$\begin{cases} \dfrac{\partial p_{\mathrm{o}}}{\partial\left(R_{\mathrm{c}}\theta\right)} = \dfrac{1}{R_{\mathrm{c}}}\dfrac{p_{\mathrm{E}} - p_{\mathrm{W}}}{2\Delta\theta}, \quad \dfrac{\partial p_{\mathrm{o}}}{\partial z} = \dfrac{p_{\mathrm{N}} - p_{\mathrm{S}}}{2\Delta z} \\ \dfrac{\partial^2 p_{\mathrm{o}}}{\left[\partial\left(R_{\mathrm{c}}\theta\right)\right]^2} = \dfrac{1}{R_{\mathrm{c}}^2}\dfrac{p_{\mathrm{E}} + p_{\mathrm{W}} - 2p_{\mathrm{o}}}{\Delta\theta^2}, \quad \dfrac{\partial^2 p_{\mathrm{o}}}{\partial z^2} = \dfrac{p_{\mathrm{N}} + p_{\mathrm{S}} - 2p_{\mathrm{o}}}{\Delta z^2} \end{cases}. \tag{S23}$$

By substituting Eq. (S23) into Eq. (S22), the first-order and second-order partial derivatives in Eq. (S22) are replaced with corresponding finite difference forms:

$$A\frac{1}{R_{\mathrm{c}}^2}\frac{p_{\mathrm{E}} + p_{\mathrm{W}} - 2p_{\mathrm{o}}}{\Delta\theta^2} + B\frac{p_{\mathrm{N}} + p_{\mathrm{S}} - 2p_{\mathrm{o}}}{\Delta z^2} + C\frac{1}{R_{\mathrm{c}}}\frac{p_{\mathrm{E}} - p_{\mathrm{W}}}{2\Delta\theta} + D\frac{p_{\mathrm{N}} - p_{\mathrm{S}}}{2\Delta z} = E. \tag{S24}$$

By rearranging Eq. (S24) , the relationship between the oil film pressure at the central node and its four adjacent nodes can be obtained:

$$\begin{aligned} &2\left(\frac{A\Delta z}{R_{\mathrm{c}}\Delta\theta} + \frac{BR_{\mathrm{c}}\Delta\theta}{\Delta z}\right)p_{\mathrm{o}} \\ &= \left(\frac{BR_{\mathrm{c}}\Delta\theta}{\Delta z} + \frac{DR_{\mathrm{c}}\Delta\theta}{2}\right)p_{\mathrm{N}} + \left(\frac{BR_{\mathrm{c}}\Delta\theta}{\Delta z} - \frac{DR_{\mathrm{c}}\Delta\theta}{2}\right)p_{\mathrm{S}} + \left(\frac{A\Delta z}{R_{\mathrm{c}}\Delta\theta} + \frac{C\Delta z}{2}\right)p_{\mathrm{E}} + \left(\frac{A\Delta z}{R_{\mathrm{c}}\Delta\theta} - \frac{C\Delta z}{2}\right)p_{\mathrm{W}} - ER_{\mathrm{c}}\Delta\theta\Delta z \end{aligned}. \tag{S25}$$

Combining Eq. (S24) and Eq. (S25), we obtain the following expressions:

$$A = \frac{h_{\mathrm{o}}^{\,3}}{\mu}, B = \frac{h_{\mathrm{o}}^{\,3}}{\mu}, C = \frac{1}{R_{\mathrm{c}}}\frac{\partial}{\partial\theta}\frac{h_{\mathrm{o}}^{\,3}}{\mu}, D = \frac{\partial}{\partial z}\frac{h_{\mathrm{o}}^{\,3}}{\mu}, \quad E = 6\left(v_\theta\frac{1}{R_{\mathrm{c}}}\frac{\partial h_{\mathrm{o}}}{\partial\theta} + v_z\frac{\partial h_{\mathrm{o}}}{\partial z} + 2\frac{\partial h_{\mathrm{o}}}{\partial t}\right). \tag{S26}$$

By substituting Eq. (S26) into Eq. (S25) and denoting α_{C}, α_{E}, α_{S}, α_{W} and α_{N} as the coefficients for the pressure at each node, and S as the constant term, the coefficients can be expressed as:

$$
\begin{cases}
\alpha_{\mathrm{N}}=\left(\dfrac{BR_{\mathrm{c}}\Delta\theta}{\Delta z}+\dfrac{DR_{\mathrm{c}}\Delta\theta}{2}\right)=\dfrac{R_{\mathrm{c}}\Delta\theta}{\Delta z}\left(\dfrac{h_{\mathrm{o}}{}^{3}}{\mu}+\dfrac{\partial}{\partial z}\dfrac{h_{\mathrm{o}}{}^{3}}{\mu}\Delta z\right)=\dfrac{R_{\mathrm{c}}\Delta\theta}{\Delta z}\dfrac{h_{\mathrm{N}}^{3}}{\mu_{\mathrm{N}}} \\
\alpha_{\mathrm{S}}=\left(\dfrac{BR_{\mathrm{c}}\Delta\theta}{\Delta z}-\dfrac{DR_{\mathrm{c}}\Delta\theta}{2}\right)=\dfrac{R_{\mathrm{c}}\Delta\theta}{\Delta z}\left(\dfrac{h_{\mathrm{o}}{}^{3}}{\mu}-\dfrac{\partial}{\partial z}\dfrac{h_{\mathrm{o}}{}^{3}}{\mu}\Delta z\right)=\dfrac{R_{\mathrm{c}}\Delta\theta}{\Delta z}\dfrac{h_{\mathrm{S}}^{3}}{\mu_{\mathrm{S}}} \\
\alpha_{\mathrm{E}}=\left(\dfrac{A\Delta z}{R_{\mathrm{c}}\Delta\theta}+\dfrac{C\Delta z}{2}\right)=\dfrac{\Delta z}{R_{\mathrm{c}}\Delta\theta}\left(\dfrac{h_{\mathrm{o}}{}^{3}}{\mu}+\dfrac{\partial}{\partial z}\dfrac{h_{\mathrm{o}}{}^{3}}{\mu}R_{\mathrm{c}}\Delta\theta\right)=\dfrac{\Delta z}{R_{\mathrm{c}}\Delta\theta}\dfrac{h_{\mathrm{E}}^{3}}{\mu_{\mathrm{E}}} \\
\alpha_{\mathrm{W}}=\left(\dfrac{A\Delta z}{R_{\mathrm{c}}\Delta\theta}-\dfrac{C\Delta z}{2}\right)=\dfrac{\Delta z}{R_{\mathrm{c}}\Delta\theta}\left(\dfrac{h_{\mathrm{o}}{}^{3}}{\mu}-\dfrac{\partial}{\partial z}\dfrac{h_{\mathrm{o}}{}^{3}}{\mu}R_{\mathrm{c}}\Delta\theta\right)=\dfrac{\Delta z}{R_{\mathrm{c}}\Delta\theta}\dfrac{h_{\mathrm{W}}^{3}}{\mu_{\mathrm{W}}} \\
\alpha_{\mathrm{C}}=2\left(\dfrac{A\Delta z}{R_{\mathrm{c}}\Delta\theta}+\dfrac{BR_{\mathrm{c}}\Delta\theta}{\Delta z}\right)=\dfrac{R_{\mathrm{c}}\Delta\theta}{\Delta z}\dfrac{h_{\mathrm{N}}^{3}}{\mu_{\mathrm{N}}}+\dfrac{R_{\mathrm{c}}\Delta\theta}{\Delta z}\dfrac{h_{\mathrm{S}}^{3}}{\mu_{\mathrm{S}}}+\dfrac{\Delta z}{R_{\mathrm{c}}\Delta\theta}\dfrac{h_{\mathrm{E}}^{3}}{\mu_{\mathrm{E}}}+\dfrac{\Delta z}{R_{\mathrm{c}}\Delta\theta}\dfrac{h_{\mathrm{W}}^{3}}{\mu_{\mathrm{W}}} \\
S=-ER_{\mathrm{c}}\Delta\theta\Delta z=-6\left(v_{\theta}\dfrac{\partial h_{\mathrm{o}}}{\partial\theta}\Delta\theta\Delta z+v_{z}\dfrac{\partial h_{\mathrm{o}}}{\partial z}R_{\mathrm{c}}\Delta\theta\Delta z+2\dfrac{\partial h_{\mathrm{o}}}{\partial t}R_{\mathrm{c}}\Delta\theta\Delta z\right) \\
\quad=-6\left[v_{\theta}(h_{\mathrm{E}}-h_{\mathrm{W}})\Delta z+v_{z}(h_{\mathrm{N}}-h_{\mathrm{S}})R_{\mathrm{c}}\Delta\theta\right]-12\displaystyle\int_{\mathrm{W}}^{\mathrm{E}}\int_{\mathrm{S}}^{\mathrm{N}}\dfrac{\partial h_{\mathrm{o}}}{\partial t}R_{\mathrm{c}}d\theta dz
\end{cases}
. \quad \text{(S27)}
$$

In Eq. (S27), $\partial h/\partial t$ represents the shifting rate of the film thickness at that location. Similar to the oil film thickness itself, the shifting rate must be specified by an initial value or the value from the previous iteration step during the Reynolds equation solution.

By using the FDM, the pressure on each node can be solved based on the linear computational equation:

$$
\alpha_{\mathrm{C}}p_{\mathrm{o}}=\alpha_{\mathrm{N}}p_{\mathrm{N}}+\alpha_{\mathrm{S}}p_{\mathrm{S}}+\alpha_{\mathrm{E}}p_{\mathrm{E}}+\alpha_{\mathrm{W}}p_{\mathrm{W}}+S\,. \quad \text{(S28)}
$$

The computational domain for solving the Reynolds equation is discretized into $n_{\mathrm{a}}\times n_{\mathrm{c}}$ grid nodes, where n_{a} and n_{c} denote the numbers of grid nodes in the axial z and circumferential θ directions, respectively. Each pressure node in the domain can be represented by the linear Eq. (S28). For nodes on the outermost boundary in the Z direction, their pressure values are equal to the boundary pressure. Starting from the boundary pressure, an iterative method is applied to solve the pressure at each node sequentially.

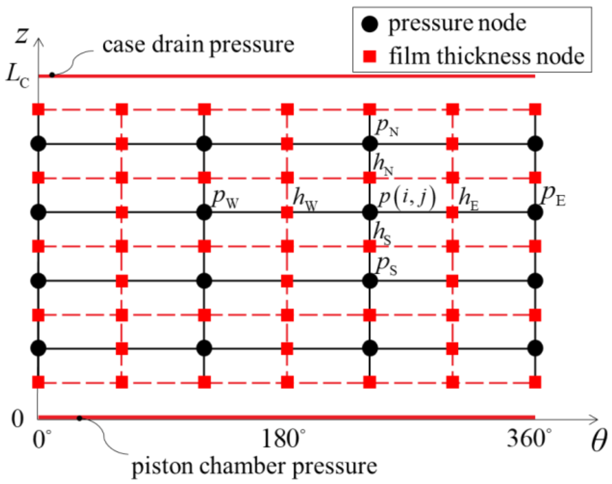

Fig. S5 Schematic Diagram of Computational Domain Grid Partitioning

Since the iterative solution of the PCI oil film starts from the pressure boundary, the values of the boundary pressure are critical. The two ends of the PCI clearance in the Z direction are connected to the piston chamber and the housing cavity, respectively. The boundary pressures are shown in Eq. (S29):

$$\begin{cases} p_{\mathrm{o}}\big|_{i=1} = p_{\mathrm{ch}} \\ p_{\mathrm{o}}\big|_{i=n_{\mathrm{a}}} = p_{\mathrm{ca}} \end{cases}, \tag{S29}$$

where p_{ch} is the piston chamber pressure, p_{ca} is the case drain pressure, typically ranging between 0.3-0.5 MPa.

Section S3 Test bench and Measurement Equipment

The APM operation was conducted on a high-speed pump test rig from The State Key Laboratory of Fluid Power and Mechatronic Systems (SKLoFP) at Zhejiang University as shown in Fig. S6. The test rig is able to operate APMs under controllable operating conditions. To precisely control the rotational speed, the tested APM is driven by an electric motor with closed-loop speed control. The outlet pressure of the APM is regulated by a relief valve in an independent hydraulic loading system. The operating condition and the specifications are consistent with Table 1.

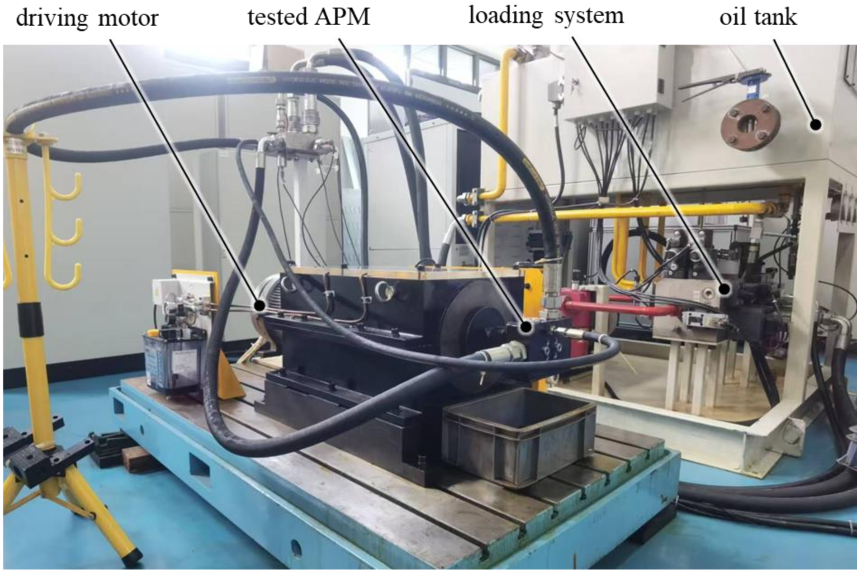

Fig. S6 High-speed pump test rig for the APM operation

The wear contour of the PCI was measured by a LEITZ PMM-C coordinate measuring machine (CMM) as shown in Fig. S7. The wear depth is generally several micrometers according to previous research (Brinkschulte et al. 2018, Lyu et al. 2020, Zhang et al. 2021, Lyu et al. 2023, Lin et al. 2024, Long et al. 2024). To verify the repeatability, a cylinder bore was measured twice by the CMM. The standard deviation of the point cloud distribution of the difference between two measurements was 0.174 μm, which is sufficient to detect the wear depth at the micrometer scale. In the surface measurement process during the wear test, circular profiles were scanned every 0.5 mm in depth to comprehensively capture the uneven wear contour of the entire cylinder bore surface. The cross section of the measurement trajectory is shown in the right part of Fig. S7, in which a coordinate system $O_{\mathrm{w}}X_{\mathrm{w}}Y_{\mathrm{w}}Z_{\mathrm{w}}$ is defined for the wear contour.

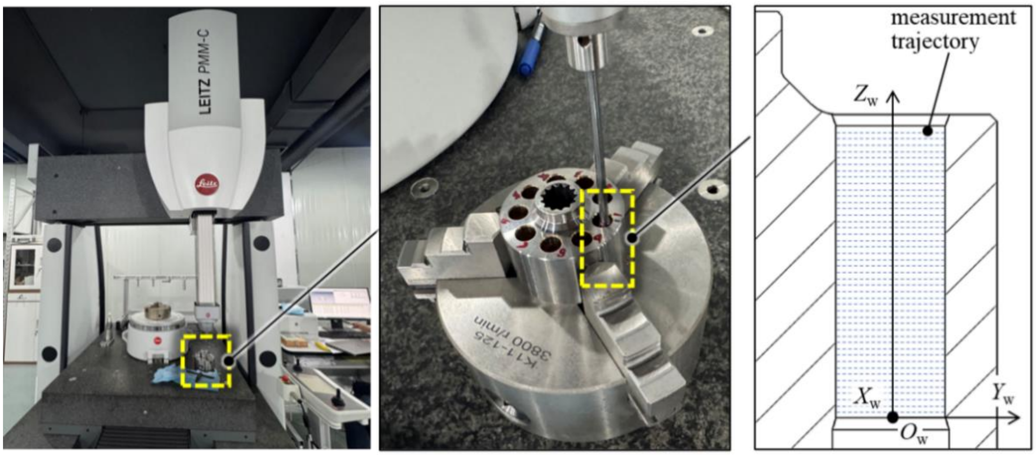

Fig. S7 Surface measurement equipment and method

References

Brinkschulte L, Mattes J, Geimer M, 2018. An approach to wear simulation of hydrostatic drives to improve the availability of mobile machines. 11th International Fluid Power Conference.

Chao Q, Zhang J, Xu B, et al., 2018. Discussion on the Reynolds equation for the slipper bearing modeling in axial piston pumps. *Tribology International*, 118:140-147.

Chu P, Cameron A, 1962. Pressure viscosity characteristics of lubricating oils. *J. Inst. Petrol*, 48(461):147.

Gohar R, Cameron A, 1967. The mapping of elastohydrodynamic contacts. *ASLE TRANSACTIONS*, 10(3):215-225.

Lin Y, Wang H, Wang H, et al., 2024. A novel wear prediction method and wear characteristic analysis of piston/cylinder pair in axial piston pump. *Wear*, 550:205402.

Long J, Lu Y, Zhang H, et al., 2024. Life cycle assessment of a slipper/swash plate friction pair based on thermal-fluid-structure lubrication state dynamic recognition. *Tribology International*, 192:109256.

Lyu F, Zhang J, Sun G, et al., 2020. Research on wear prediction of piston/cylinder pair in axial piston pumps. *Wear*, 456:203338.

Lyu F, Zhang J, Zhao S, et al., 2023. Coupled evolution of piston asperity and cylinder bore contour of piston/cylinder pair in axial piston pump. *Chinese Journal of Aeronautics*, 36(8):395-407.

Mizell D, 2018. A Study of the Piston Cylinder Interface of Axial Piston Machines. PhD Thesis, Purdue University, West Lafayette, USA.

Patir N, Cheng H, 1978. An average flow model for determining effects of three-dimensional roughness on partial hydrodynamic lubrication. *Journal of Tribology*, 100(1):12-17.

Ransegnola T, Shang L, Vacca A, 2022. A study of piston and slipper spin in swashplate type axial piston machines. *Tribology International*, 167:107420.

Sarode S, Shang L, Vacca A, 2022. Numerical investigation of the influence of part geometric tolerances on piston/cylinder interface performance. *International Journal of Fluid Power*, 23(3):343-362.

Singh K, Sadeghi F, Russell T, et al., 2021. Fluid–structure interaction modeling of elastohydrodynamically lubricated line contacts. *Journal of Tribology*, 143(9):091602.

Zhang J, Lyu F, Xu B, et al., 2021. Simulation and Experimental Investigation on Low Wear Rate Surface Contour of Piston/Cylinder Pair in an Axial Piston Pump. *Tribology International*, 162:107127.